PLUG-IN HYBRID ELECTRIC VEHICLE POWER MANAGEMENT: OPTIMAL CONTROL AND BATTERY SIZING

by

Scott J. Moura

A thesis submitted in partial fulfillment
of the requirements for the degree of
Masters of Science and Engineering
(Mechanical Engineering)
in The University of Michigan
2008

Masters Committee:

Professor Jeffrey L. Stein, Co-Chair
Assistant Research Scientist Hosam K. Fathy, Co-Chair
Assistant Research Scientist Duncan S. Callaway, Co-Chair

ACKNOWLEDGMENTS

I would like to acknowledge my girlfriend, Jovauna Currey, whose love and support was instrumental in making this thesis possible.

I would also like to express gratitude to my research advisors, Dr. Hosam Fathy, Dr. Duncan Callaway, and Professor Jeffrey Stein. Their supportive mentoring and probing questions not only aided the completion of this thesis, but helped me become a better research scientist. When I entered graduate school at the University of Michigan, Hosam joked that I was "as green as green can be" with regard to performing research. As I look back, I am truly amazed by how much they have taught me.

The financial support necessary to complete this work was made possible through the generous contributions of the Rackham Graduate School and National Science Foundation, under the Rackham Merit Fellowship and Graduate Student Research Fellowship, respectively.

My fellow labmates, Tulga Ersal, Rahul Ahlawat, Ben Pence, and Joel Forman provided key feedback on this project, through individual discussions and group lab meetings. I wish to thank them for their constructively critical questions and moral support.

Finally, I want to thank the love and support of my parents, Manny and Bonnie Moura. I cannot imagine two better role models for parents. Their life stories are a testament to the fact that hard work and persistence will enable you to achieve your dreams.

Contents

Abstract

This thesis examines plug-in hybrid electric vehicles (PHEVs), i.e. automobiles that can extract power from either chemical fuels or stored electricity, in which the latter is typically regenerated by plugging into the electric grid. This research contains two goals. First, it develops power management algorithms that optimize the way a PHEV splits power demand among its various, and often redundant, actuators. Optimal power management enables PHEVs to attain improved fuel economy and operating cost levels while maintaining battery pack health. Furthermore, the optimal "blending" of fuel and electricity usage in a PHEV provides significant economic benefits to vehicle owners, especially for certain fuel-to-electricity price ratios. Secondly, the thesis evaluates the impact of varying battery size on the performance and efficiency of our previously developed power management algorithms. Specifically, our aim is to determine the extent to which power management algorithm choice can enable the use of smaller batteries, while retaining certain cost and performance characteristics, over distributions of trip duration and drive cycle trajectories.

The first part examines the problem of optimally splitting driver power demand among the different actuators (i.e., the engine and electric machines) in a plug-in hybrid electric vehicle (PHEV). The current state of art optimizes PHEV power management for fuel economy, subject to charge sustenance constraints, over individual drive cycles. This paper adds three original contributions to this literature. First, it uses stochastic dynamic programming to optimize PHEV power management over a distribution of drive cycles, rather than a single cycle. Second, it explicitly trades off fuel and electricity usage in a PHEV, thereby systematically exploring the potential benefits of controlled charge depletion over aggressive charge depletion followed by charge sustenance. Finally, it examines the impact of variations in relative fuel-to-electricity pricing on optimal PHEV power management. The results provided herein focus on a single-mode power-split PHEV configuration for mid-size sedans, but the approach is general to other configurations and sizes as well.

The second part builds on the first by establishing a framework for assessing and quantifying the performance tradeoffs between battery size and control algorithm choice. In particular, it rigorously analyzes operating costs and efficiency using two different control strategies explicitly optimized for certain battery sizes within a finite set. Existing studies examine this effect for power management algorithms derived using either rule-based or deterministic dynamic programming methods. The approach presented here extends research on PHEV battery energy capacity to PHEVs that use power management algorithms identified with stochastic dynamic programming. Futhermore, it treats both PHEV trip duration and PHEV power demand as stochastic functions informed by drive cycle data and travel surveys. The results indicate that a blending strategy enables the use of smaller battery sizes for a broad range of energy price ratios. However, the benefits diminish with increasing battery size and rising fuel-to-electricity price ratios. As a result, our analysis demonstrates how optimal control algorithms can reduce battery cost and potentially catalyze the

market penetration of PHEVs.

Chapter 1

A Stochastic Optimal Control Approach for Power Management

1.1 Introduction

This section examines plug-in hybrid electric vehicles (PHEVs), i.e., automobiles that can extract propulsive power from chemical fuels or stored electricity, and can obtain the latter by plugging into the electric grid. The section's goal is to develop power management algorithms that optimize the way a PHEV splits its overall power demand among its various, and often redundant, actuators. Such optimal power management may help PHEVs attain desirable fuel economy and emission levels with minimal performance and drivability penalties [1], [2]. Furthermore, the optimal "blending" of fuel and electricity usage in a PHEV may also provide significant economic benefits to vehicle owners, especially for certain fuel-to-electricity price ratios [3].

The literature provides a number of approaches to hybrid vehicle power management, many equally applicable to both plug-in and conventional (i.e., non plug-in) hybrids. These approaches all share a common goal, namely, to meet overall vehicle power demand while optimizing a metric such as fuel/electricity consumption, emissions, or some careful combination thereof. For example, the equivalent fuel consumption minimization approach [4–6] uses models of electric powertrain performance to mathematically convert electricity consumption to an equivalent amount of fuel, and then makes real-time power split decisions to minimize net fuel consumption. The manner in which most approaches optimize vehicle performance is either by identifying a power management trajectory, or by establishing a power management rule base. Trajectory power management algorithms require knowledge of future power demand and use this information to specify the future power output of each actuator. Such optimization can be performed offline for drive cycles known a priori using deterministic dynamic programming (DDP) [7–10], and can also be performed

online using optimal model predictive control [11], [12]. Rule-based approaches, in comparison, constrain the power split within a hybrid vehicle to depend only on the vehicle's current state and input variables (e.g., vehicle/engine speed, battery charge, power demand, etc.) through some map, or rule base [13–19]. One then tailors this rule base to ensure that each actuator in the powertrain operates as close to optimally as possible. These maps can be constructed from engineering expertise and insight, or using more formal methods such as optimization [17] or fuzzy logic [18], [19]. Stochastic dynamic programming (SDP) methods are particularly appealing in this context, despite their well-recognized computational complexity [20], because of their ability to optimize a power split map for a probabilistic distribution of drive cycles, rather than a single cycle [21–25].

The above survey briefly examines the hybrid power management literature for both plug-in and conventional hybrid electric vehicles. Within the specific context of PHEVs, power management research has generally focused on fuel economy improvement, subject to constraints on battery state of charge, using either the rule-based [16], [17] or DDP approach [9], [10]. This section extends this research by adding three important original contributions to the PHEV power management literature. First, it uses SDP to optimize PHEV power management over a probability distribution of drive cycles. Second, it explicitly accounts for the interplay between fuel and electricity costs in PHEV power management. This makes it possible, for the first time, to fully explore the potential benefits of controlled charge depletion over aggressive charge depletion followed by charge sustenance. Finally, this chapter presents what the authors believe to be the first study on the impact of variable electricity and petroleum purchase prices on optimal PHEV power management. The above contributions are made specifically for a single-mode power-split PHEV configuration, although the approach is extendible to other configurations as well.

The remainder of this section is organized as follows: Section 1.2 introduces the vehicle configuration, problem definition, and vehicle model. Section 1.3 then describes the numerical optimization method adopted in this work. Section 1.4 discusses the results of this optimization, and Section 1.5 highlights the chapter's key conclusions.

1.2 Problem Formulation

Figure 2.1 portrays the main components and configuration of the powertrain architecture considered in this thesis, often called the single-mode power split, "series/parallel", or "combined". This architecture combines internal combustion engine power with power from two electric motor/generators (identified as M/G1 and M/G2) through a planetary gear set. The planetary gear set creates both series and parallel paths for power flow to the wheels. The parallel flow paths (dashed blue arrows) include a path from the engine to the wheels and a path from the battery, through the motors, to the wheels. The series flow path, on the other hand, takes power from the engine to the battery first, then back through the electrical system to the wheels (solid

red arrows). This redundancy of power flow paths, together with battery storage capacity, increases the degree to which one can optimize powertrain control for performance and efficiency while meeting overall vehicle power demand.

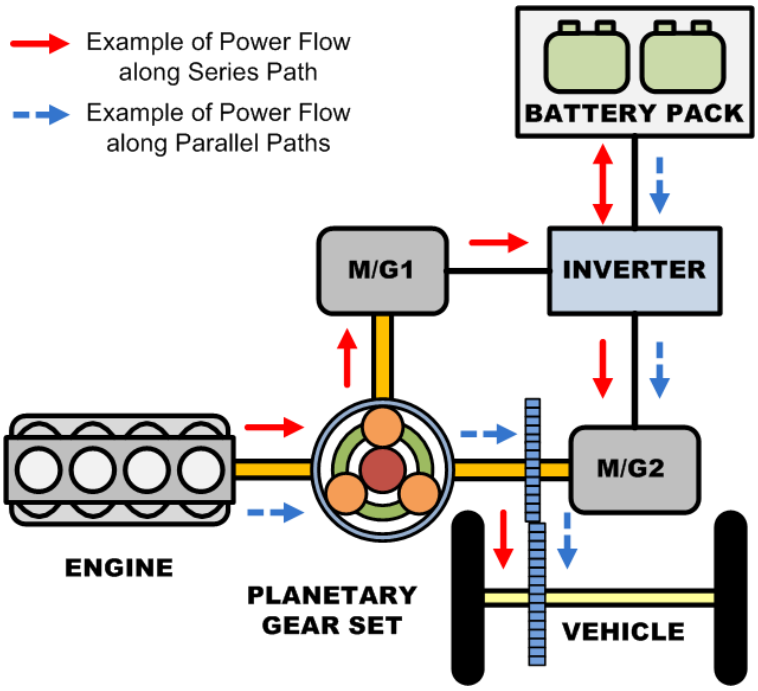

Figure 1.1: The single mode power-split hybrid architecture uses a planetary gear set to split power amongst the engine, M/G1, and M/G2. Diagram adapted from [26].

The above power split hybrid vehicle architecture can be used for a variety of vehicle sizes and needs. This thesis focuses on a midsize sedan power split PHEV whose key component sizes are listed in Table I. This PHEV is quite similar in configuration, dynamics, and design to the 2002 Toyota Prius, but with roughly twice the battery capacity. Specifically, we assume that the PHEV has 80 modules of Ni-MH batteries instead of 38 in the 2002 Prius. This choice of battery size and type is partly motivated by the relative ease with which one can convert the above conventional hybrid vehicle into an experimental PHEV - by simply adding Ni-MH battery energy capacity. Chapter 2 builds on this chapters's results by examining the influence of battery sizing on the optimal control laws studied herein [27]. Furthermore, the impact of battery type (e.g., Lithium-ion vs. Ni-MH, etc.) on PHEV performance and efficiency is the subject of Chapter 2.

Given the above vehicle, powertrain, and battery choices, this thesis examines the following power management problem:

$$\text{Minimize}: \qquad J = \lim_{N\to\infty} \mathrm{E}_{P_{dem}} \left[\sum_{k=0}^{N-1} \gamma^k g(x(k), u(k)) \right] \tag{1.1}$$

$$\text{Subject} \quad \text{to}: \qquad \begin{aligned} x(k+1) &= f(x(k), u(k)) \\ x &\in X \\ u &\in U \end{aligned} \tag{1.2}$$

In this discrete-time stochastic optimal control problem, k represents an arbitrary discrete time instant, and the sampling time is 1 second. This sampling time is consistent with the project's focus on supervisory, rather than servo, control. The optimization objective in this control problem consists of the instantaneous combined cost of PHEV fuel and electricity consumption, $g(x(k), u(k))$, accumulated over time, discounted by a constant factor γ, and averaged over the stochastic distribution of instantaneous power demand, P_{dem}. In optimizing this objective, we impose three important constraints, namely, (i) the PHEV powertrain's dynamics, represented by $f(x(k), u(k))$, (ii) the set of admissible PHEV states, X, and (iii) the set of admissible control inputs, U. The remainder of this section presents these optimization objectives and constraints in more detail. Specifically, Sections II-A through II-D present, respectively, the PHEV model $f(x(k), u(k))$, the optimization functional $g(x(k), u(k))$, the state and control constraint sets X and U, and the Markov chain-based drive cycle model used for computing the expected PHEV optimization cost.

1.2.1 PHEV Model

To model the dynamics of a PHEV, we first identify the PHEV's inputs, outputs, and state variables. Towards this goal, Figure 2.2 presents a conceptual map of the key interactions between the PHEV examined in this thesis, its human driver, and its supervisory power management algorithm. This conceptual map adopts the fairly common tradition in hybrid power management research of interpreting the driver's accelerator and brake pedal positions as a power signal, P_{dem}, demanded at the wheels (e.g., [22–24]). The supervisory power management algorithm attempts to meet this power demand by adjusting three control input signals: engine torque T_e, M/G1 torque $T_{M/G1}$, and M/G2 torque $T_{M/G2}$. Engine startup and shutdown can also be treated as a control input, but this thesis assumes, for simplicity, that the PHEV engine idles when power is not demanded. This leaves the important issue of engine startup/shutdown, and its complex impact on PHEV warm-up and emissions, as open topics for ongoing research. In summary, therefore, the PHEV plant has three control inputs, namely, the three engine/motor/generator torques.

The above control inputs affect the PHEV plant by affecting its state variables. In this thesis, we closely follow some of the existing hybrid vehicle power management research by choosing engine crankshaft speed ω_e, longitudinal vehicle velocity v, and battery state of charge SOC, as the three PHEV state variables [23]. We use a Markov memory variable to represent the stochastic distribution of driver power demand, as explained in Section II-D.

To model the dynamics governing the PHEV state variables, we begin by expressing the total road load,

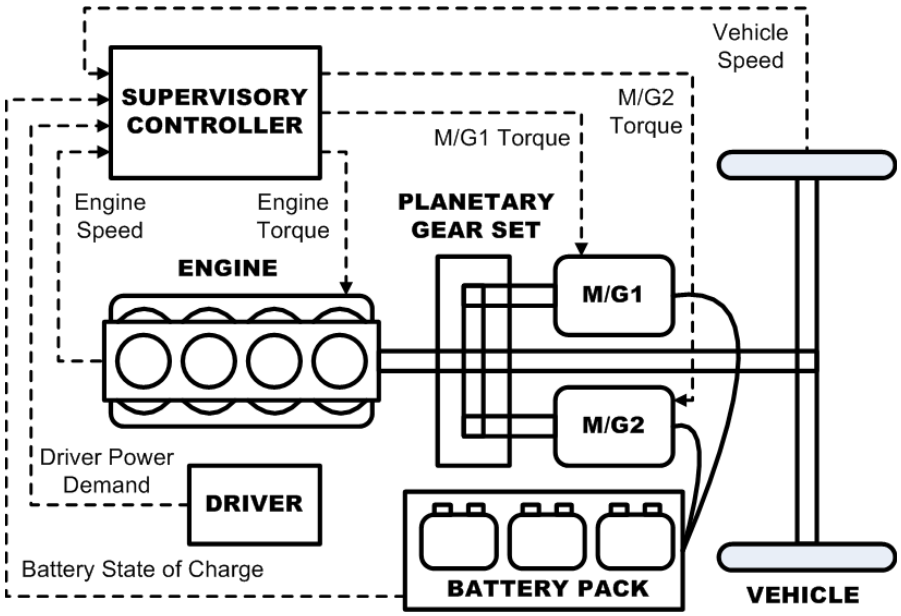

Figure 1.2: PHEV model components and signal flow. Note that the signal flow forms a state feedback control architecture.

F_{road}, acting on the PHEV as follows:

$$F_{road} = F_{roll} + F_{drag} + F_{damp} \tag{1.3}$$

In this equation, F_{roll} is a rolling resistance term given by:

$$F_{roll} = \mu mg \tag{1.4}$$

where g, m, and μ represent the acceleration of gravity, mass of the PHEV, and a rolling resistance coefficient (assumed constant), respectively. Furthermore, F_{drag} is an aerodynamic drag force given by:

$$F_{drag} = 0.5\rho A_{fr} C_d v^2 \tag{1.5}$$

where ρ , A_{fr} and C_d represent the density of air, the PHEV's effective frontal area, and the PHEV's effective aerodynamic drag coefficient, respectively. Finally, F_{damp} is a wheel/axle bearing friction term given by:

$$F_{damp} = \frac{b_w v}{r_{tire}} \tag{1.6}$$

where b_w is the bearing's damping coefficient and r_{tire} is an effective PHEV tire radius. Note that this expression for wheel damping, as well as other derivations below, assumes a direct proportionality between wheel angular velocity and vehicle speed, where the proportionality constant is related to the tire radius and final drive ratio. This assumption effectively neglects tire slip for simplicity, thereby eliminating the need for using two separate state variables to represent wheel and vehicle speeds.

Road loads from (1.3) act on the PHEV powertrain through the planetary gear set sketched in Fig. 1.3. This planetary gear set can be conceptually and mathematically treated as an ideal "lever" connecting the engine, two motor/generators, and vehicle wheels (through the final drive), as shown in Fig. 1.3. Using this lever diagram in conjunction with Euler's equations of motion, one can relate the road load in (1.3) to angular velocities in the PHEV powertrain as follows [23]:

$$\begin{bmatrix} I_e & 0 & 0 & R+S \\ 0 & I_{M/G1} & 0 & -S \\ 0 & 0 & I'_{M/G2} & -R \\ -(R+S) & S & R & 0 \end{bmatrix} \begin{bmatrix} \dot{\omega}_e \\ \dot{\omega}_{M/G1} \\ \dot{\omega}_{M/G2} \\ F \end{bmatrix} = \begin{bmatrix} T_e \\ T_{M/G1} \\ T'_{M/G2} \\ 0 \end{bmatrix} \tag{1.7}$$

In this equation, R and S denote the numbers of teeth on the planetary gear set's ring and sun, respectively. The angular velocities of the engine and two motor/generators are denoted by ω_e, $\omega M/G1$, and $\omega_{M/G2}$, respectively. Furthermore, T_e and I_e denote the engine's brake torque and inertia, and $T_{M/G1}$ and $I_{M/G1}$ denote the torque and inertia of the first motor/generator, respectively. The force F represents an internal reaction force between the planetary gear set's sun and planet gears. Finally, the terms $I'_{M/G2}$ and $T'_{M/G2}$ are effective inertia and torque terms given by:

$$\begin{aligned} I'_{M/G2} &= I_{M/G2} + (I_w + m r_{tire}^2)/K^2 \\ T'_{M/G2} &= T_{M/G2} - F_{road} r_{tire}/K \end{aligned} \tag{1.8}$$

where $I_{M/G2}$ and I_w are the rotational inertias of the second motor/generator and wheel, K is the final drive gear ratio, and $T_{M/G2}$ is the torque produced by the second motor/generator.

The point-mass model in (1.7) and (1.8) provides a complete description of how the state variables ω_e and v (which is directly proportional to $\omega_{M/G2}$) evolve with time for given control input trajectories. This description is provided in differential algebraic equation (DAE) form, with the force F and velocity $\omega_{M/G1}$ acting as dependent state variables. Simple algebraic manipulations, omitted herein, can be used in conjunction with time discretization to convert this DAE description to the explicit form in (1.2).

To complete the derivation of the PHEV plant model, we assume for simplicity that the PHEV's battery can be idealized as an open-circuit voltage V_{oc}, in series with some internal resistance R_{batt}. We allow both V_{oc} and R_{batt} to depend on battery state-of-charge, SOC, through a predefined map (adapted from [28], [29]). Furthermore, we define SOC as the ratio of charge stored in the battery to some known maximum charge capacity, Q_{batt}. This furnishes the following relationship between the rate of change of SOC and the current I_{batt}, generated by the battery:

$$\dot{SOC} = -I_{batt}/Q_{batt} \tag{1.9}$$

To obtain an expression for the current, I_{batt}, we note that the instantaneous power delivered by the

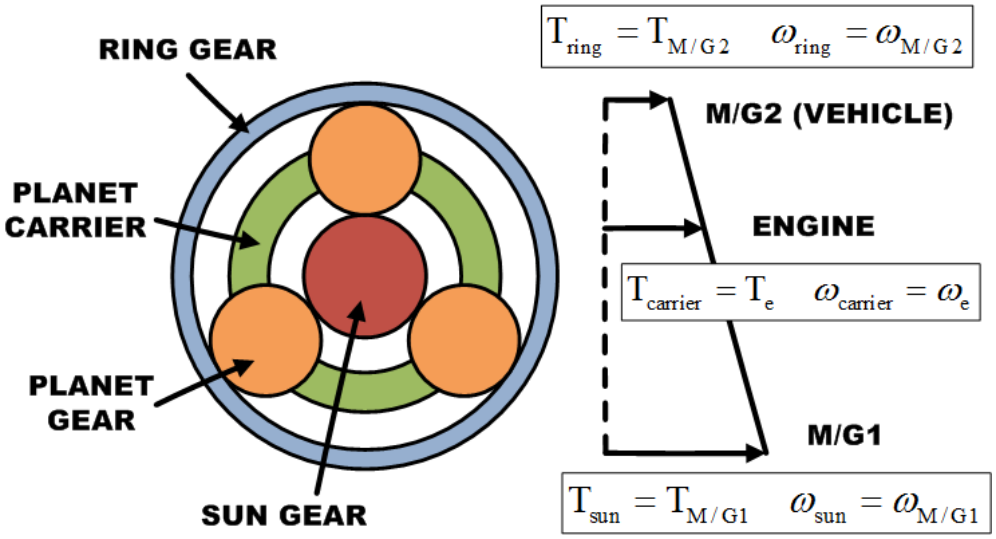

Figure 1.3: Planetary gear set and lever diagram. The engine, M/G1, and M/G2 are attached to the planet carrier, sun, and ring gears, respectively.

battery to the two motor/generators, P_{batt}, is related to I_{batt} through the following power balance:

$$P_{batt} = V_{oc} I_{batt} - R_{batt} I_{batt}^2 \tag{1.10}$$

Solving (1.9) and (1.10) for the rate of change of SOC gives:

$$\dot{SOC} = -\frac{V_{oc} - \sqrt{V_{oc}^2 - 4P_{batt}R_{batt}}}{2Q_{batt}R_{batt}} \tag{1.11}$$

Finally, relating the power P_{batt} to the torques, speeds, and efficiencies of the two motor/generators gives:

$$P_{batt} = T_{M/G1}\omega_{M/G1}\eta_{M/G1}^{k_{M/G1}} + T_{M/G2}\omega_{M/G2}\eta_{M/G2}^{k_{M/G2}} \tag{1.12}$$

where

$$k_i = \begin{cases} -1 & T_i\omega_i > 0 \\ 1 & T_i\omega_i \leq 0 \end{cases} \quad \text{for} \quad i = \{M/G1, M/G2\} \tag{1.13}$$

Combining (1.11)-(1.13) with maps from [28], which relate the efficiencies of the electric motor/generators to their torques and speeds, provides a complete description of the battery SOC dynamics as a function of PHEV states and inputs. Discretizing this description and combining it with an explicit discretized form of (1.7) and (1.8) furnishes a complete model of the PHEV plant dynamics, i.e., $f(x(k), u(k))$ in (1.2). This model mostly replicates existing hybrid powertrain models in the literature (e.g., [23]), but we use it in conjunction with the novel objective function in Section II-B to examine PHEV power management.

1.2.2 Objective Function

The optimization objective, J, in (1.1) aggregates the expected combined cost of PHEV fuel and electricity consumption over a stochastic distribution of trips, and discounts this cost exponentially through the factor γ. This discount factor, if restricted to the interval $[0, 1)$, ensures that the cumulative optimization objective remains finite over infinite time horizons. This research follows Lin [22] in setting γ to 0.95, leaving the question of how different values of γ affect optimal PHEV power management open for future research.

To explicitly trade off fuel and electricity consumption in PHEVs, we define the instantaneous cost functional, namely, $g(x(k), u(k))$ in (1.1), as follows:

$$g(x, u) = \beta\alpha_{fuel}W_{fuel} + \alpha_{elec}\frac{1}{\eta_{grid}}P_{elec} \tag{1.14}$$

The first term in this cost functional quantifies PHEV fuel consumption, while the second term quantifies electricity consumption, and the coefficient β makes it possible to carefully study tradeoffs between the two. Specifically, W_{fuel} represents the fuel consumption rate in grams per time step, where we use the engine map in [28] to convert engine torque and speed to fuel consumption. The constant parameter α_{fuel} then converts this rate to an energy consumption rate, in megajoules (MJ) per time step. Similarly, P_{elec} represents the instantaneous rate of change of the battery's internal energy, i.e.,

$$P_{elec} = -V_{oc}Q_{batt}S\dot{O}C \tag{1.15}$$

The constant parameter α_{elec} converts P_{elec} to MJ per time step. Dividing this change in stored battery energy by a constant charging efficiency $\eta_{grid} = 0.98$ (which corresponds to a full recharge in six hours) furnishes an estimate of the amount of energy needed from the grid to replenish the battery charge consumed during the trip. Note that P_{elec} is positive when the PHEV uses stored battery energy and negative during regeneration. Hence, there exists a reward for regeneration that offsets the need to consume grid electricity. The magnitude of this reward depends on the parameter β, which represents the relative price of gasoline per MJ to the price of grid electricity per MJ. We refer to this parameter as the "energy price ratio," and use it to examine the tradeoffs between fuel consumption and electricity consumption in PHEVs. Specifically, we begin this chapter's power management optimization studies by setting a price ratio of $\beta = 0.8$, consistent with the average energy prices in 2006, namely \$2.64 USD per gallon of gasoline and \$0.089 USD per kWh of electricity [30]. We then vary this ratio to examine the influence of different relative fuel-to-electricity prices on optimal power management, as shown in Section IV-C.

1.2.3 Constraints

In optimizing PHEV power management, we seek controllers capable of keeping the state vector x within simple bounds expressed as a constraint set X in (1.16). These bounds ensure that the engine neither

exceeds its maximum allowable speed nor falls to speeds where noise, vibrations, and harshness (NVH) become excessive [26]. They also constrain battery state of charge to remain between two limits denoted as $SOC_{min} = 0.25$ and $SOC_{max} = 0.9$. Constraining SOC in such a way helps to protect against capacity and power fade due to over-charging or excessive discharging [10], [16], [17]. However, the precise impact of the depths and rates of PHEV battery charging/discharging on battery health is still under investigation. Finally, we also impose limits on the speeds of the motor/generators to protect them from damage. As explained in Section III-B, when solving the optimal PHEV power management problem numerically, we use exterior point penalty functions to implement all of these state constraints as "soft" constraints [31].

$$X = \left\{ x : \begin{array}{c} \omega_{e,min} \leq \omega_e \leq \omega_{e,max} \\ \omega_{M/G1,min} \leq \omega_{M/G1} \leq \omega_{M/G1,max} \\ \omega_{M/G2,min} \leq \omega_{M/G2} \leq \omega_{M/G2,max} \\ SOC_{min} \leq SOC \leq SOC_{max} \end{array} \right\} \tag{1.16}$$

In addition to constraining the PHEV state variables, we also implement two types of control input constraints as part of power management optimization: a drivability constraint and control input bounds. The drivability constraint, given by (1.17), ensures that driver power demand is met by equating it to the sum of the three engine/motor/generator power outputs:

$$P_{dem} = P_e + P_{M/G1} + P_{M/G2} \tag{1.17}$$

Since the power output of each PHEV actuator equals its torque multiplied by its angular velocity, which depends directly on the PHEV's states, this constraint reduces the number of independent control inputs from three to two. The choice of which two torque commands to make independent is arbitrary, but we select engine torque and M/G1 torque to match existing work [23]. Hence, the vector of independent control inputs becomes:

$$u = \begin{bmatrix} T_e & T_{M/G1} \end{bmatrix}^T \tag{1.18}$$

As with the state variables, we constrain the two elements of this vector to take values within an admissible control set denoted by $U(x)$ in (1.19). This control set limits the rate of battery charging and discharging to minimize battery damage, and also limits the engine and motor/generator torque to safe and attainable values. We refer to control policies that map states to control inputs within this set as "admissible" policies [20].

$$U(x) = \left\{ u : \begin{array}{c} \omega_{e,min} \leq T_e \leq T_{e,max} \\ T_{M/G1,min} \leq T_{M/G1} \leq T_{M/G1,max} \\ T_{M/G2,min} \leq T_{M/G2} \leq T_{M/G2,max} \\ P_{chg,lim} \leq P_{batt} \leq P_{dis,lim} \end{array} \right\} \tag{1.19}$$

1.2.4 Drive Cycle Modeling

The drive cycle model is a stochastic component to the plant model which predicts the distribution of future power demands using a discrete-time Markov chain [32]. Specifically, the model defines a probability of reaching a certain power demand in the next time step, given the power demand and vehicle speed in the current time step [22]. To acquire a numerical realization of this model, we define a state space for the Markov chain by selecting a finite number of power demand and vehicle speed samples. Then we form an array of conditional transition probabilities according to:

$$p_{i,j,m} = \Pr\left(P_{dem}(k+1) = i | P_{dem}(k) = j, v(k) = m\right) \tag{1.20}$$

where i,j index power demand and m indexes vehicle speed. To estimate these transition probabilities, one needs observation data for both power demand and vehicle speed. We obtain these observations from a number of drive cycle profiles. The profiles provide histories of vehicle speed versus time, and we invert the PHEV dynamics to extract corresponding power demand histories. This results in the following equation for power demand, solely in terms of vehicle velocity and vehicle parameters:

$$P_{dem} = m\frac{dv}{dt}v + \frac{1}{2}\rho A_{fr} C_d v^3 + \mu m g v + b_w v^2 / r_{tire} \tag{1.21}$$

In this work, we used federal drive cycles (FTP-72, US06, HWFET) and real-world micro trips (WVUCITY, WVUSUB, WVUINTER) in the ADVISOR database [28] to compute the observation data. We then derived the transition probabilities in (1.20) from this data using maximum likelihood estimation [33].

1.3 Stochastic Dynamic Programming

This section presents the stochastic dynamic programming approach used for solving the optimal power management problem posed in Section II. The approach begins with a uniform discretization of the admissible state and control input sets, X and $U(x)$. This discretization makes the optimal power management problem amenable to computer calculations, but generally produces suboptimal results. We use the symbols X and $U(x)$ to refer to both the continuous and discrete-valued state and control input sets for ease of reading. Given the discrete-valued sets, we apply a modified policy iteration algorithm [20] to compute the optimal power management cost function and policy. This algorithm consists of two successive steps, namely, policy evaluation and policy improvement, repeated iteratively until convergence. For each possible PHEV state, the policy iteration step approximates the corresponding "cost-to-go" J, which may be intuitively interpreted as the expected cost function value averaged over a stochastic distribution of drive cycles starting at that state. The policy improvement step then approximates the optimal control policy u^*, corresponding to each

possible PHEV state. This process iterates, as shown in Fig. 1.4, until convergence. Sections III-A and III-B present the policy iteration and policy improvement steps in further detail.

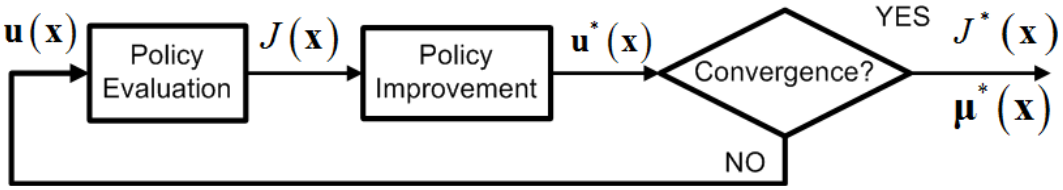

Figure 1.4: Modified policy iteration flowchart. The process consists of two successive steps, policy evaluation and policy improvement, repeated iteratively until a convergence criterion is satisfied.

1.3.1 Policy Evaluation

The policy evaluation step computes the cost-to-go for each state vector value, x, given a control policy, $u(x)$. This computation is performed recursively as shown in (1.22):

$$J_{n+1}(x) = g(x,u) + \mathrm{E}_{P_{dem}}\left[\gamma J_n(f(x,u))\right] \tag{1.22}$$

The index n in the above *recurrence relation* represents an iteration number, and the recurrence relation is evaluated iteratively for all state vector values in the discretized set of admissible states, X. In general, the cost-to-go values within the expectation operator must be interpolated because $f(x,u)$ will not always generate values in the discrete-valued state set X. Although the true cost-to-go for a given control policy must satisfy $J_n = J_{n+1}$, we iterate (1.22) a finite number of times before executing the policy improvement step (next section). This truncated policy evaluation approach, used in combination with the policy improvement step below, converges to the optimal control policy regardless of the maximum number of iterations [20].

1.3.2 Policy Improvement

Bellman's principle of optimality indicates that the optimal control policy for the stochastic dynamic programming problem in (1.1) and (1.2) is also the control policy that minimizes the cost-to-go function $J(x)$ in (1.22). Thus, to find this control policy u^*, we minimize cost-to-go with respect to this policy for each state vector value x, given the cost-to-go function $J(x)$. Mathematically, this minimization is represented by:

$$u^*(x) = \arg\min_{u \in U(x)} \left\{ g(x,u) + \mathrm{E}_{P_{dem}}[\gamma J(x)] + g_{cons}(x) \right\} \tag{1.23}$$

Equation (1.23) imposes the state and control input set constraints from (1.2) in the form of an exterior point quadratic penalty term [31], $g_{cons}(x)$. This penalty term consists of sixteen penalty functions summed together, each corresponding to one of the inequalities given in (1.16) and (1.19). Each penalty function

equals the excursion from the corresponding constraint boundary, normalized with respect to the feasible range of operation, squared, and multiplied by a coefficient five orders of magnitude greater than the energy consumption weights. For example, the penalty function for minimum engine speed takes the form:

$$g_{cons,\omega_{e,min}} = \alpha_{cons,\omega_{e,min}} \left[\min \left\{ 0, \frac{\omega_{e,min} - \omega_e}{\omega_{e,max} - \omega_{e,min}} \right\} \right]^2 \tag{1.24}$$

After both policy evaluation and policy improvement are completed, the optimal control policy is passed back into the policy evaluation step and the entire procedure is repeated iteratively. The process terminates when the infinity norm of the difference between two consecutive steps is less than 1%, for both the cost and control functions.

1.4 Results and Discussion

This section analyzes the properties of the proposed PHEV power management approach by comparing its performance against a baseline control policy, inspired by previous research [1], [16], [17]. Specifically, it is fairly common in PHEV power management research to examine algorithms that initially operate in a *charge depletion* mode, then switch to *charge sustenance* once some minimal battery state of charge is reached [1], [16], [17]. The charge depletion mode typically utilizes stored battery energy to meet as much of the driver power demand as possible (engine power may be needed when demand exceeds the power capabilities of the motor/generators), thereby depleting battery charge rapidly. The charge sustenance mode then uses engine power to regulate battery state of charge once it reaches some predefined minimum. This *charge depletion, charge sustenance* (CDCS) approach implicitly assumes that fuel consumption dominates operating costs relative to electricity consumption from the battery. We implement CDCS in this work by setting α_{elec} in (1.14) to zero and rely on the minimum SOC constraint in (1.16) to enforce charge sustenance behavior once battery charge is depleted. We refer to power management strategies that are the result of setting all coefficients in (1.14) to nonzero values as *blended*, since a weighted sum of both electricity and fuel is utilized to construct the power split map.

In the remainder of this section, we first analyze the performance of the blended and CDCS strategies by focusing on two FTP-72 drive cycles simulated back-to-back. Second, we examine the difference between these two control strategies in more depth by exploring how they manage engine speed and torque. Finally, we investigate the impact of varying fuel and electricity purchase prices on the optimal blended and CDCS control laws.

1.4.1 Performance

To illustrate the potential performance improvements of a blending strategy over a CDCS strategy, consider their responses for two FTP-72 drive cycles simulated back-to-back, as shown in Fig. 1.5 and 1.6. The total cost of energy for this trip is 6.4% less for the blended strategy relative to CDCS, and fuel consumption is reduced by 8.2%. Blending accomplishes this by utilizing the engine more during the charge depletion phase, thereby assisting the battery to meet total power demand more often than CDCS. Although in the blended case the engine operates at higher loads, therefore consuming more fuel, the engine efficiency is greater and, as demonstrated in Fig. 1.6, battery charge depletes more slowly. As a result, blending and CDCS incur nearly the same total energy costs through the depletion phase (Fig. 1.5), and the advantage of blending in terms of overall cost arises from its delayed entry into charge sustenance.

The benefit of delayed entry into charge sustenance is evident from previous research in the literature in which the PHEV drive cycle and total trip length were assumed to be known *a priori* (e.g., [9], [16]). For example, in [9] deterministic dynamic programming furnished blending strategies that reached minimum SOC exactly when the PHEV trip terminated, thereby never allowing the PHEV to enter the charge sustenance mode. This result agrees with our current findings, namely, that the primary benefit of blending strategies results from their ability to delay or eliminate the need for charge sustenance. However, the approach in [9] requires knowledge of trip length *a priori*. Since SDP explicitly takes into account a probability distribution of drive cycle behavior, our identified strategy is optimal in the average sense.

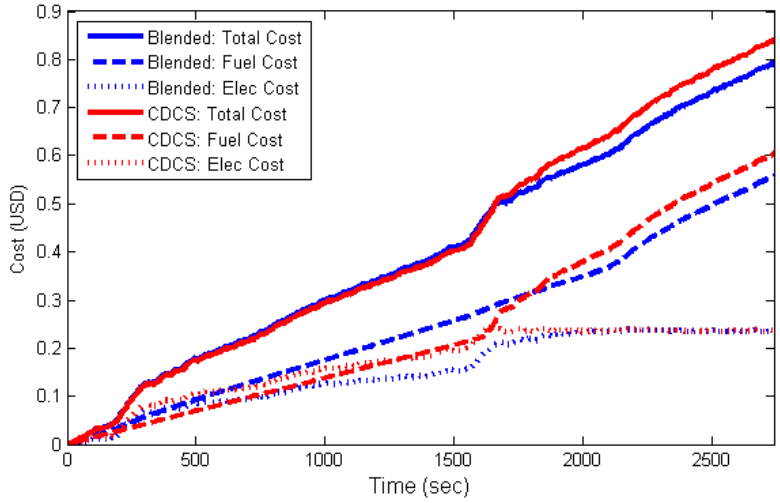

Figure 1.5: Running energy consumption costs for blended and CDCS control strategies on two FTP-72 cycles simulated back-to-back. The total cost (solid line) is the sum of fuel (dashed line) and electricity (dotted line) costs.

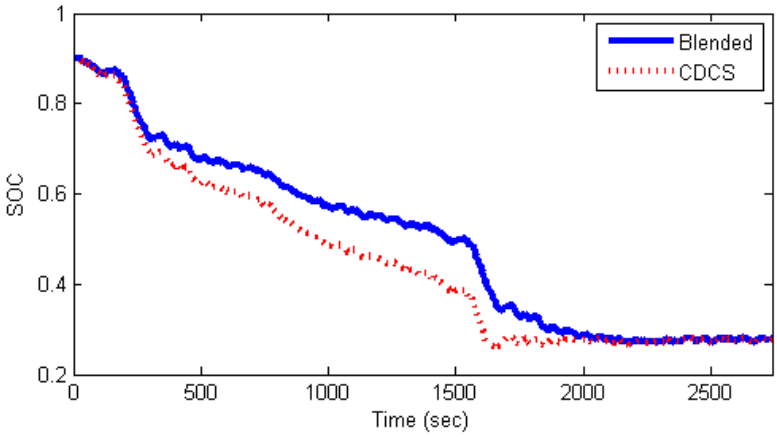

Figure 1.6: State-of-charge response for blended and CDCS control strategies on two FTP-72 cycles simulated back-to-back.

Performance improvements of blending over CDCS are uniform across all the drive cycles shown in Table II, where the drive cycle lengths are selected to ensure that the vehicle reaches charge sustenance before the trip terminates. If the vehicle reaches its destination before entering charge sustenance phase, however, the total energy consumption costs are nearly identical for blending and CDCS (as demonstrated in Fig. 1.5). Therefore the blending strategy proposed herein has no significant energy consumption cost penalty for early trip termination. Note that some of the largest improvements are observed for drive cycles that were not used to estimate the Markov state transition probability matrix.

1.4.2 Engine Control

A significant benefit of the power-split architecture is the fact that it decouples the engine crankshaft from the road, and allows the electric machines to move engine speed where fuel efficiency is maximized [**?**]. This optimal operating line is identified by the black dashed line in Fig. 1.7 and 1.8. As shown in Fig. 1.7, the blending strategy initially operates the engine at fairly low speeds and high torques, close to the optimal fuel efficiency operating line. This occurs even when power demand can be met by the electric motors alone. The excess engine power goes towards regenerating battery charge, which the blended cost function in (1.14) rewards. Moreover, the electric machines are not generally saturated and are thus free to maintain low engine speeds and high efficiencies. In contrast, the CDCS strategy causes the engine to remain at very low brake torque levels during depletion, where fuel consumption is low but so is engine efficiency (Fig. 1.8). Moreover, significant power is requested from the engine only when the electric machines saturate and cannot meet driver power demand by themselves. This limits the control authority of the electric machines when driver power demand is large, thereby reducing their ability to move engine speed to the optimal operating line.

These observations explain how the blending strategy utilizes the engine and electric motors more efficiently, thereby delaying the charge sustenance phase and improving overall PHEV operating costs.

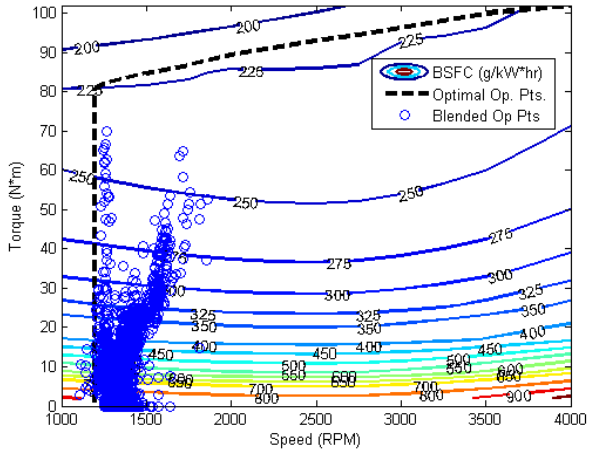

Figure 1.7: Engine operating points for the blended strategy on a brake specific fuel consumption map, for two FTP-72 cycles simulated back-to-back.

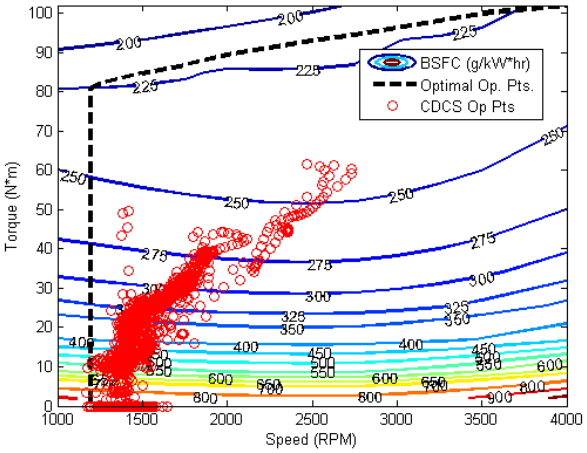

Figure 1.8: Engine operating points for the CDCS strategy on a brake specific fuel consumption map, for two FTP-72 cycles simulated back-to-back.

1.4.3 Energy Price Ratio

An important feature of the proposed power management algorithm is its dependence on the energy price ratio, β , which varies temporally (e.g., by year) and spatially (e.g., by geographic region). To investigate the nature of this dependence, we obtained the history of energy price ratios since 1973 [30], shown in Fig. 1.9. The value of β has clearly changed significantly over the past 35 years due to shifts in both oil and electricity prices. This motivates the need to understand how this parameter impacts optimal PHEV power management.

Consider the SOC depletion responses shown in Fig. 10 for controllers synthesized with energy price ratios in the set $\beta \in 0.4, 0.6, 0.8, 1.0, 1.2$ and for a CDCS strategy, which by definition does not depend on β. Several conclusions can be drawn from this parametric study. First, as β approaches infinity (i.e. fuel becomes infinitely more expensive than grid electric energy), the optimal blending strategy converges to a CDCS strategy. This is consistent with the fact that the CDCS strategy implicitly assumes the cost of fuel is infinitely more than the cost of electricity. Secondly, for sufficiently low β (i.e. electricity becomes more expensive than fuel), the optimal blending strategy generates electric energy. The implicit assumption leading to this result is that the driver is able to sell energy back to the grid when the vehicle is plugged in. Although electricity prices are unlikely to be this high in general, real-time pricing could motivate using

the vehicle as a distributed power generator during periods of peak demand when conventional generation is scarce [34]. This suggests that, with the appropriate exchange of information, a vehicle could be configured to modify its control policy in real time to reflect grid conditions. Hence, our proposed controller is extendible toward vehicle-to-grid infrastructures.

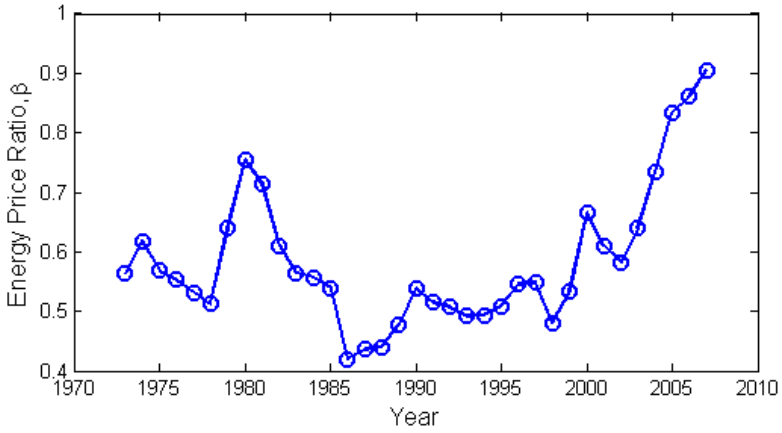

Figure 1.9: Historic values for the energy price ratio β from 1973 to 2007 [30]. Note how the variation corresponds with shifts in oil and electricity prices.

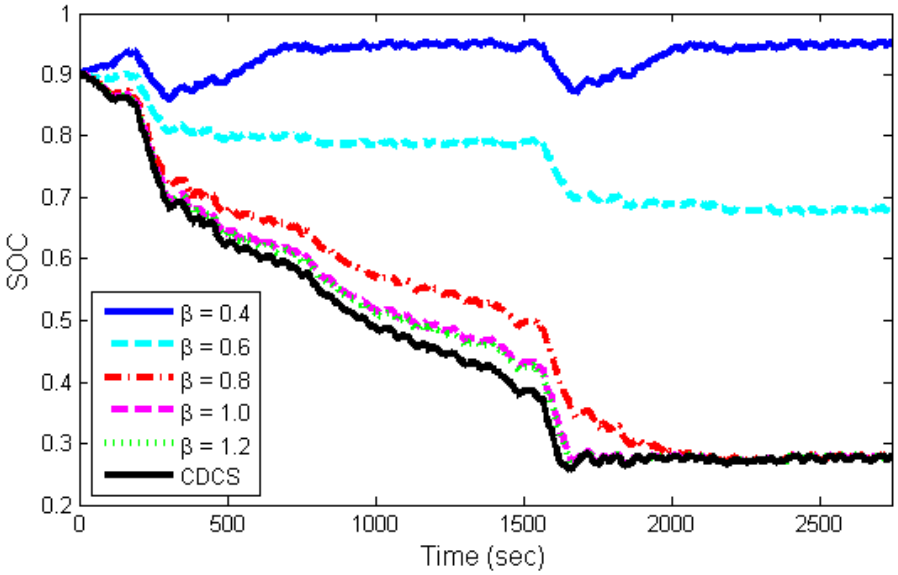

Figure 1.10: State-of-charge response for varying β (blended) and CDCS control strategies on two FTP-72 cycles simulated back-to-back. Blending approaches CDCS as β approaches infinity.

1.5 Conclusions

This chapter demonstrates the use of stochastic dynamic programming for optimal PHEV power management. It derives an optimal power management strategy that rations battery charge by blending engine and battery power in a manner that improves engine efficiency and reduces total charge sustenance time. This strategy explicitly takes into account a probability distribution of drive cycles and variable energy price ratios. This formulation guarantees a solution that is optimal in the average sense, without requiring drive cycle knowledge *a priori*. Moreover, we have shown that energy price ratios can significantly influence the characteristics of the optimal control policy. Indeed, it may be useful to equip production PHEVs with a range of control laws corresponding to the range of price ratios that could be experienced over the life of the vehicle.

Chapter 2

Interplay of Battery Sizing and Optimal Power Management

2.1 Introduction

This chapter examines plug-in hybrid electric vehicles (PHEVs), which typically utilize onboard battery storage to at least partially displace liquid fuels with less expensive grid electricity. Battery sizing and design plays a key role in the cost, reliability, and ability of such PHEVs to effectively manage different power demand levels over the course of a diverse set of trip durations [3]. The goal of this chapter is examine the interplay between battery storage capacity and PHEV power management, specifically by quantifying the extent to which different PHEV power management algorithms enable the use of smaller batteries without compromising performance and efficiency. This quantification focuses on two power management algorithms: one that minimizes fuel consumption, and one that optimally blends fuel and electricity usage. The performance and efficiency characteristics of these algorithms are compared for different battery sizes over stochastic distributions of drive cycle trajectories and trip durations.

Previous work has investigated PHEV battery sizing from several different perspectives, including drive cycle requirements [35–37] and control design [9, 16, 37]. The results of this research show that existing battery technologies possess the power-to-energy characteristics necessary to achieve all-electric ranges of up to 60km, at least for U.S. federally mandated drive cycle trajectories (e.g., FTP-72, HWFET, US06) [35], [36]. However, the literature also shows that operating PHEVs in an all-electric battery depletion mode often requires batteries with both high energy and high power characteristics, thus resulting in more expensive components [16,35–37]. This motivates the use of smaller batteries in combination with "*blending*" control strategies that utilize engine power throughout the depletion process to ration battery energy and

reduce electric power requirements by shifting load to the combustion engine. In O'Keefe and Markel [9], PHEV power management was explicitly optimized for fuel consumption over some known drive cycle using deterministic dynamic programming (DDP), for two different PHEVs (one with sufficient electric power capacity to meet all power demand, and one with half as much power capacity). This optimization furnished a control trajectory that blends battery and fuel usage such that the minimum battery energy level is achieved exactly when the trip terminates, and the "half sized" PHEV had nearly the same fuel economy as the full size PHEV for trips over a certain length.

This chapter provides two new contributions to this body of literature. First, it builds on previous work by the authors [38] to study PHEV battery performance using stochastic drive cycle models developed by combining the Markov chain modeling framework with real-world data distributions of daily travel duration. Secondly, it analyzes the monetary cost, efficiency, and battery discharge depth of PHEVs over a distribution of daily drive cycles, thereby establishing the machinery for a rigorous study on the tradeoffs between battery size and PHEV performance. Finally, in contrast to the work referenced in the previous paragraph, which generally focuses on blending as a means to reduce power capacity requirements for the electric drive train, here we study the impact that blending can have on the energy storage requirements of the vehicle. The chapter's results indicate that a blending strategy enables the use of batteries with less storage capacity, thus complementing previous research that demonstrates the benefits of blending for reducing PHEV power requirements.

The remainder of the chapter is organized as follows: Section 2.2 introduces the vehicle configuration and models for the PHEV, daily travel time distributions, and drive cycles. Section 2.3 describes the simulation approach, and Section 2.4 presents the main results and discusses the impact of battery size and control strategy on expected trip cost, expected efficiency, and state-of-charge range. The chapter's conclusions are provided in Section 2.4.

2.2 PHEV Model and Power Management Algorithm

This chapter analyzes a hybrid vehicle model based upon the single mode power-split (a.k.a. parallel/series or combined) hybrid architecture in Fig. 2.1. The key benefit of the power-split design is that it possesses energy flow characteristics of both parallel and series configurations. The parallel flow paths include engine-to-wheels and battery-to-wheels (blue arrows), while the series flow path is from the engine-to-battery-to-wheels (red arrows). The role of the planetary gear set is to manage energy flow between these paths by transferring mechanical power between the engine, two motor/generators (identified as M/G1 and M/G2), and the wheels [26]. An interesting result of this arrangement is that, with the appropriate control strategy, power can be split amongst the three paths to optimize energy consumption.

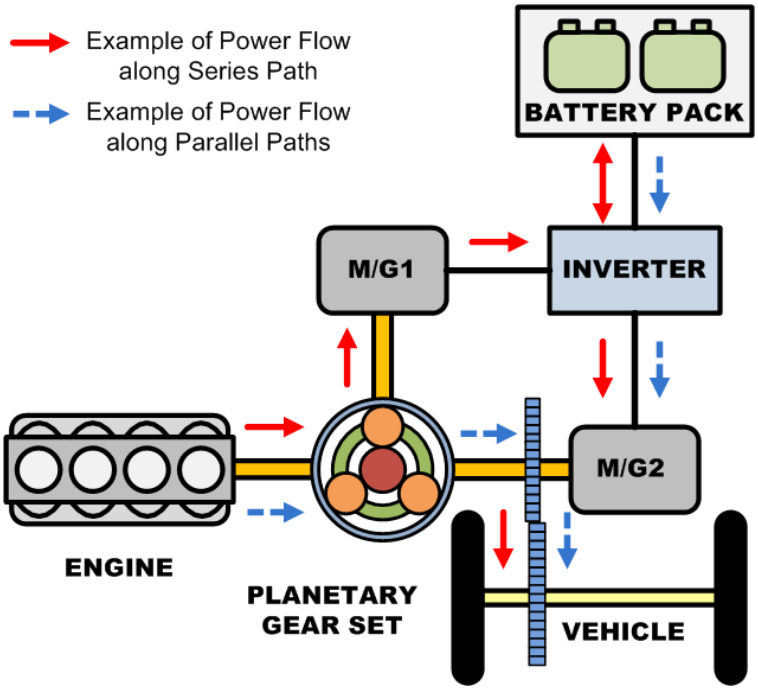

Figure 2.1: The single mode power-split hybrid architecture uses a planetary gear set to split power amongst the engine, M/G1, and M/G2. Diagram adapted from [26].

2.2.1 PHEV Model

The vehicle model used in this thesis, summarized below and described in detail in [38], is based upon existing research on conventional hybrid electric vehicles (HEVs) [23], [22], [24]. The planetary gear set model utilizes Euler's Law to describe the inertial dynamics of the engine and motor/generators [23]. The engine and motor/generator models are steady-state maps, which relate speed and torque to fuel consumption and power efficiency [28].

Although lithium-ion (Li-ion) batteries are being strongly considered for PHEV applications, in this chapter we choose to model nickel-metal hydride (NiMH) batteries for several reasons. First, they are widely used in current HEVs and therefore their performance characteristics are better understood that Li-ion. Second, some early production PHEVs may utilize NiMH batteries [39]. Finally, the general objective of blending in this chapter is to make more efficient use of the battery and engine, and since this principle carries over to Li-ion technology, we expect our results to be generalizable.

Each NiMH cell within the battery pack is modeled by an equivalent circuit comprising an ideal voltage source $V_{oc,cell}$ in series with an Ohmic resistor R_{cell} [23], [29], where each cell has a charge capacity of Q_{cell}. Both the open circuit voltage and internal resistance are functions of battery state of charge (SOC) taken from steady-state maps available in [22]. These equivalent circuits are assembled in a series-parallel

combination to model the entire battery pack, where n_s denotes the number of cells in series per parallel string, n_p denotes the number of parallel strings, and the total number of cells in the pack is $n_s n_p$. The open circuit voltage V_{oc}, internal resistance R, and charge capacity Q for the entire battery pack are given by:

$$V_{oc} = n_s V_{oc,cell} \quad R = \frac{n_s}{n_p} R_{cell} \quad Q = n_p Q_{cell} \tag{2.1}$$

The battery pack dynamics are associated with SOC, which intuitively describe a battery "fuel gauge". Here, we define SOC as the ratio of charge to maximum charge. As a result, the derivative of SOC is the ratio of current through the circuit I to an estimated maximum charge capacity Q.

$$\dot{SOC} = -I/Q \tag{2.2}$$

Through applying power conservation on the equivalent circuit, we obtain an expression for battery power at the terminals in (2.3), which is simply open circuit power less resistive losses. This expression may be written in terms of SOC using (2.2) and solved using the quadratic formula to obtain an ordinary differential equation for SOC in (2.4).

$$P_{batt} = V_{oc} I - R I^2 \tag{2.3}$$

$$\dot{SOC} = -\frac{V_{oc} - \sqrt{V_{oc}^2 - 4 P_{batt} R}}{2QR} \tag{2.4}$$

Note that the battery model is scalable with respect to the number of cells. Although this formulation explicitly accounts for series-parallel cell architectures, it can be mathematically shown that, holding $n_s n_p$ constant, the SOC dynamics are invariant to n_s and n_p individually. We will use this fact to avoid the need to specify the cell architecture. In practice, of course, pack voltage, inverter efficiency, heat generation, charge equalization, and state of health must all be considered in the battery design process [40], [41].

The states for the assembled PHEV plant model include engine crankshaft speed ω_e, longitudinal vehicle velocity v, battery state of charge SOC, and driver power demand P_{dem}. The controlled inputs to the plant include engine torque T_e, M/G1 torque $T_{M/G1}$, and M/G2 torque $T_{M/G2}$. Figure 2.2 shows that the state and control signals form a state feedback control loop around the PHEV model components.

2.2.2 Power Management Algorithm

In previous work we developed optimal power management algorithms that minimize the combined consumption cost of fuel and electricity [38]. As in other work [22–24], [21], [25], these control strategies can be implemented without prior knowledge of the trip characteristics, other than a stochastic power demand model. Mathematically, the optimal control problem is summarized in the following infinite horizon formulation:

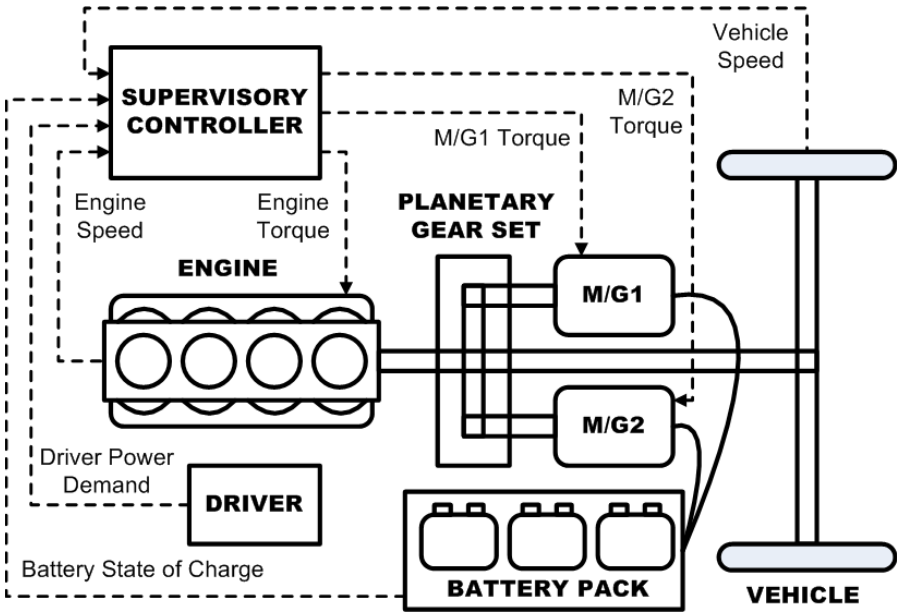

Figure 2.2: PHEV model components and signal flow. Note that the signal flow forms a state feedback control architecture.

$$\text{Minimize}: \qquad J = \lim_{N\to\infty} \mathrm{E}_{P_{dem}} \left[\sum_{k=0}^{N-1} \gamma^k g(x(k), u(k)) \right] \tag{2.5}$$

$$\text{Subject to}: \qquad \begin{array}{c} x(k+1) = f(x(k), u(k)) \\ x \in X \\ u \in U \end{array} \tag{2.6}$$

$$p_{i,j,m} = \Pr\left(P_{dem}(k+1) = i | P_{dem}(k) = j, v(k) = m\right) \tag{2.7}$$

$$P_{dem} = P_e + P_{M/G1} + P_{M/G2} \tag{2.8}$$

$$x \in X = \left\{ x : \begin{array}{c} \omega_{e,min} \le \omega_e \le \omega_{e,max} \\ \omega_{M/G1,min} \le \omega_{M/G1} \le \omega_{M/G1,max} \\ \omega_{M/G2,min} \le \omega_{M/G2} \le \omega_{M/G2,max} \\ SOC_{min} \le SOC \le SOC_{max} \end{array} \right\} \tag{2.9}$$

$$u \in U(x) = \left\{ u : \begin{array}{c} \omega_{e,min} \leq T_e \leq T_{e,max} \\ T_{M/G1,min} \leq T_{M/G1} \leq T_{M/G1,max} \\ T_{M/G2,min} \leq T_{M/G2} \leq T_{M/G2,max} \\ P_{chg,lim} \leq P_{batt} \leq P_{dis,lim} \end{array} \right\} \tag{2.10}$$

where $g(x(k), u(k))$ is the energy consumption cost per time step k and γ is the discount factor. The optimization is subject to both deterministic (2.6) and stochastic (2.7) model dynamics. The stochastic dynamics (2.7) take the form of a first order Markov chain in which P_{dem} is the Markov state variable [22]. The constraint (2.8) ensures power demand is always met by the power sources. In (2.9) and (2.10), X is the set of admissible state values x, and U is the set of admissible control values u. The time step is one second. We use this framework to develop two separate control strategies, "blended" and "charge-depletion, charge sustenance" (CDCS), defined as follows:

Blended: The blended approach minimizes a weighted sum of fuel consumption and electric energy consumption

$$g(x, u) = \beta \alpha_{fuel} W_{fuel} + \alpha_{elec} \frac{1}{\eta_{grid}} P_{elec} \tag{2.11}$$

The parameter β, which we refer to as the "energy price ratio," represents the price of gasoline per megajoule (MJ) relative to the price of electricity per MJ. The conversion factors α_{fuel} and α_{elec} are selected to convert energy consumption from each source to common units of MJ per time step. W_{fuel} is the fuel consumption rate in terms of grams per time step, and P_{elec} is power flow through the battery, which can be calculated from the battery pack open-circuit voltage, charge capacity and $\dot{SOC}$.

$$P_{elec} = -V_{oc} Q_{batt} \dot{SOC} \tag{2.12}$$

Note that P_{elec} is positive for discharge events and negative for regeneration events. We estimate the electric energy consumed from the grid during the recharge process by dividing P_{elec} by a constant charging efficiency $\eta_{grid} = 0.98$, which corresponds to a full recharge in six hours. For the main set of results in this chapter we assume a fuel price ratio of $\beta = 0.8$, which roughly corresponds to 2006 gas and electricity prices in the U.S. [30]. However, we will also briefly report on results for other price ratios, and leave a more detailed analysis for a future publication.

CDCS: It is common in PHEV power management research to use control laws that first deplete the battery as quickly as possible to a low SOC and then enter a charge sustenance mode like those used by conventional HEVs [37], [16], [1], [17]. This method, which we shall refer to as charge depletion-charge sustenance (CDCS), is implemented in the SDP framework here by setting α_{elec} in (2.11) equal to zero, thus degenerating into formulations suggested by [22–24], [25].

2.2.3 Trip Duration Model

We model trip duration as a random variable T, whose distribution gives the total travel time for a vehicle during a single day, which we treat as the travel time between PHEV charging events. This model is based on data from the 2001 National Household Travel Survey (NHTS) conducted by the Department of Transportation Federal Highway Administration [30]. Figure 2.3 shows the distribution of surveyed daily vehicle travel times, for which the mean is approximately 35 minutes and 75 percent of daily travel occurs in 32 minutes or less. The likely cause of the data's multi-modality is a tendency among survey participants to report trip duration in 5 minute increments. Since our intent is to randomly generate trip durations by inverting the trip duration cumulative distribution function (cdf), we compute the cdf and attenuate the modes with a five minute, uniformly weighted moving average in Fig. 2.4.

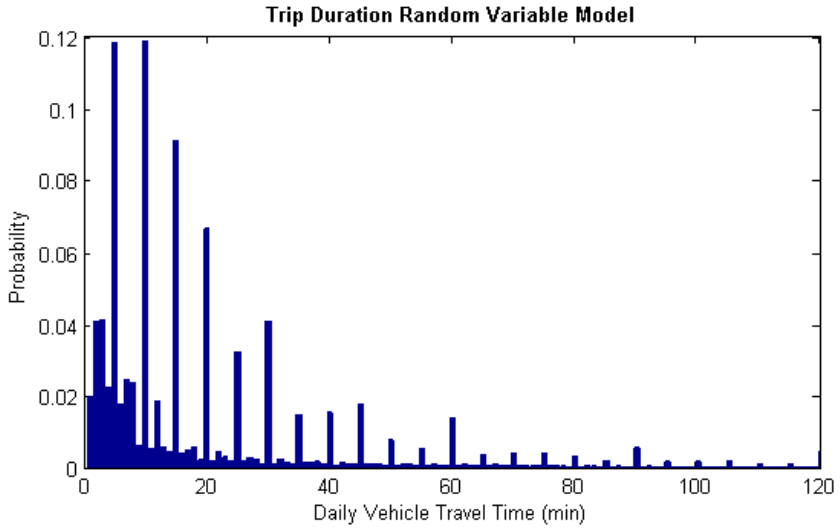

Figure 2.3: Distribution of daily vehicle travel times from 2001 NHTS.

2.2.4 Drive Cycle Model

Drive cycle trajectories are modeled via a first order Markov chain, where power demand P_{dem} is the Markov state variable. This approach to modeling drive cycle trajectories is used widely in the hybrid vehicle power management literature [38], [22–24], [21], [21]. The transition probabilities for the Markov chain given by (2.7) are determined using a maximum-likelihood estimator [33] from observation data collected from federal drive cycles (FTP-72, HWFET, US06) and real-world micro-trips (WVUCITY, WVUSUB, WVUINTER) in the ADVISOR database [28]. An example randomly generated drive cycle is shown in Fig. 2.5. The Markov model assumes that the current state is conditioned only on the state immediately preceding it. We validated this assumption by computing the model residuals and confirming that their autocorrelation

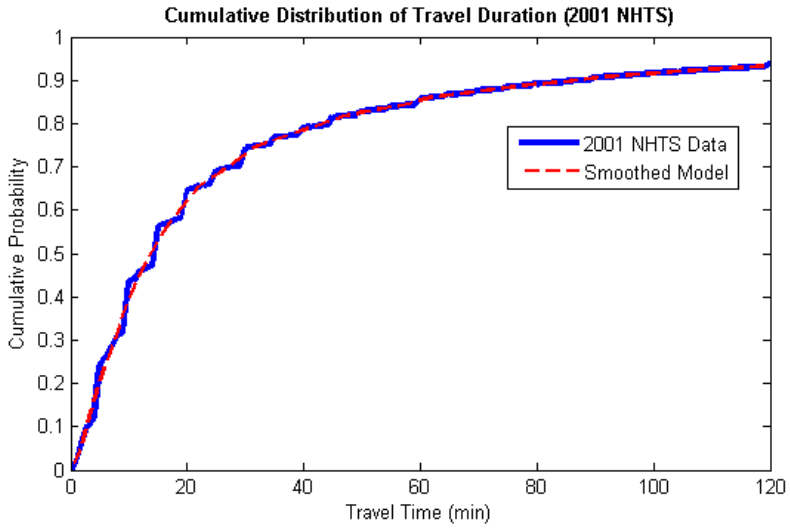

Figure 2.4: Cumulative distribution of daily vehicle travel times. The smoothed model is generated by a five minute uniformly weighted moving average of the original data.

exceeds the 95 percent confidence interval for no more than 5 percent of all lag values that are 25% of the length of the data set or less - as is the case for a white noise process [42].

In the simulation method described below, we will assume that trip duration and the Markov model are independent. Although this is clearly an important assumption, there is limited data to test its validity, and we will leave it to future work to address the sensitivity of our results to the presence of drive cycle / trip duration dependence (e.g. longer trips tend to take place on the highway).

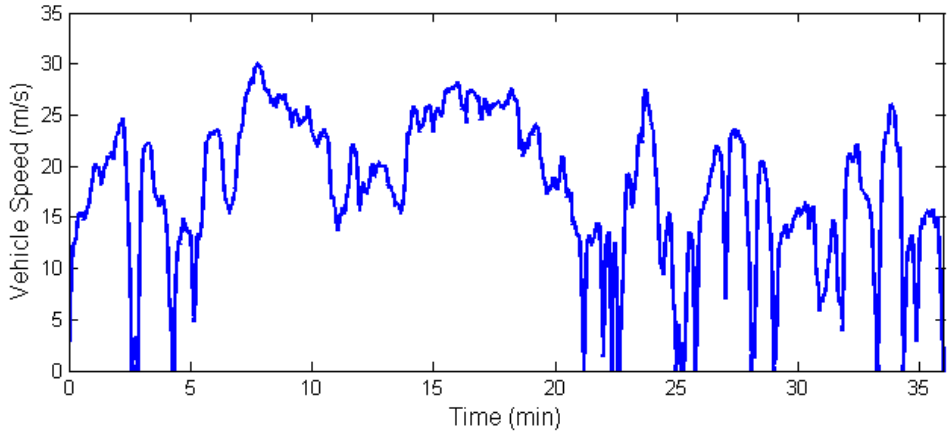

Figure 2.5: A sample randomly generated drive cycle from the Markov chain model.

2.3 Simulation Method

Distributions for the PHEV performance characteristics are calculated by simulating each control strategy (Blended and CDCS) and battery size (Table II) configuration over the entire distributions of trip duration and drive cycles. For each battery size option, we identify both a blended and CDCS control law (as explained in Section II-B and [38]). We then evaluate the performance of the control law / battery size combination by the following approach:

1. Sample a trip duration from the cdf in Figure 2.4.
2. Generate a power demand time series from the Markov chain model (2.7) with duration found in step 1.
3. Simulate the PHEV model on this randomly generated drive cycle and record the performance characteristics.
4. Check the stopping criterion (Appendix). If satisfied, stop simulations. If not satisfied, return to step 1.

2.4 Results and Discussion

2.4.1 Operating Costs & Efficiency

Figures 2.6 and 2.7 show the distribution of operating costs (in USD per km) and energy efficiency (in MJ per km) for each battery size and control strategy configuration we examined. For each battery size we see that the distribution of operating costs and energy efficiency is consistently better for the blended strategy than for CDCS. The figure suggests that the blended strategy can achieve a given level of performance with fewer battery modules than a CDCS control policy. This is especially true for smaller batteries. For batteries with more than 160 modules, the difference between the two control strategies diminishes. This can be explained by the fact that trips rarely end after a 160-plus module battery is fully depleted, for either strategy, and the two strategies are roughly cost-equivalent during the charge depletion phase [38]. These results are in agreement with prior claims that a blended strategy should enable the use of smaller batteries [35], [37], [16], although in this case the result applies to battery energy capacity, whereas the prior claims are predominantly in reference to battery power capacity.

It is important to note that the results shown here are for an energy price ratio of $\beta = 0.8$. As demonstrated in our previous work [38], the blended strategy converges to CDCS for very high price ratios. We re-ran the simulations shown in Fig. 2.6 and 2.7 for $\beta = 2.0$ and found that, while we observe no penalty for using the blended strategy, the CDCS and blended distributions begin to converge for small battery sizes as

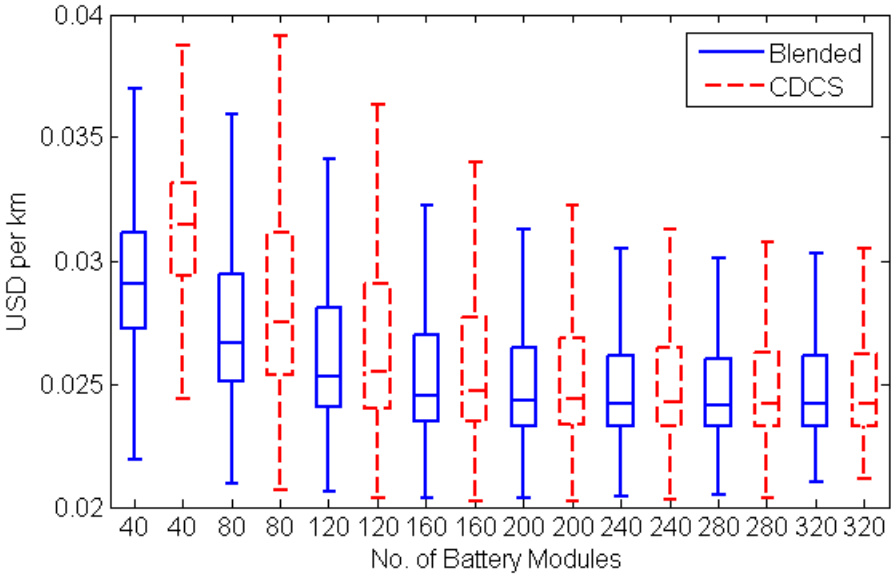

Figure 2.6: Box and whisker plots of operating cost (USD per km) for each battery size and control strategy configuration. Whisker lengths are limited to 1.5 times the interquartile range.

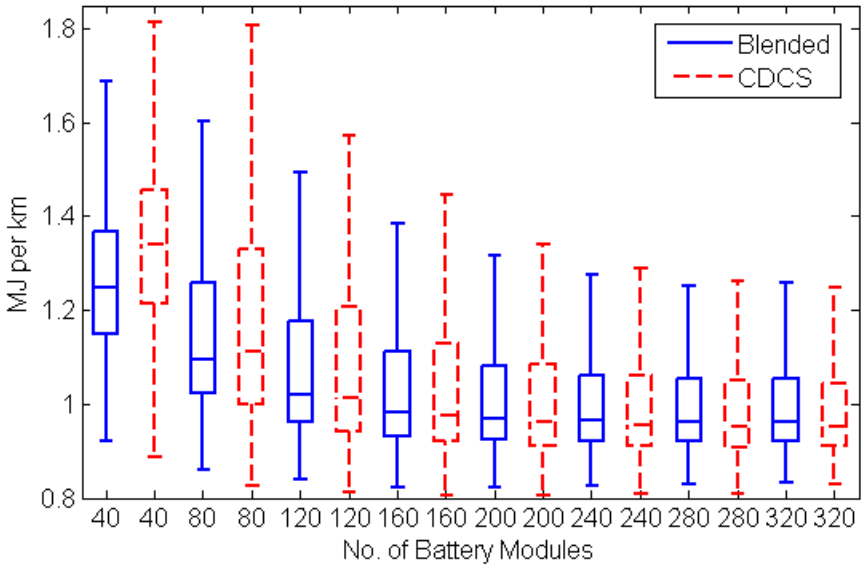

Figure 2.7: Box and whisker plots of energy efficiency (MJ per km) for each battery size and control strategy configuration. Whisker lengths are limited to 1.5 times the interquartile range.

well. These results suggest that although the blended strategy provides diminishing benefits as β increases, it remains appropriate for all β.

The asymptotic nature of the cost and efficiency of both control strategies implies that there are diminishing returns to increasing battery size. This result is directly related to the trip duration distribution: for very large battery sizes (greater than 200 modules), it is unlikely that the battery will fully deplete its charge because the bulk (75%) of daily trip durations are less than 35 minutes. Instead, the power management algorithm remains in charge depletion mode, where blending and CDCS achieve nearly equal operating costs, as demonstrated in our previous research [38]. For extremely long travel durations, however, CDCS enters charge sustenance mode before the blending strategy and quickly accumulates elevated operating costs. This is the reason why the largest observations (upper whiskers in Fig. 2.6 and 2.7) for CDCS are consistently larger than the largest observations for blending.

We expect that this phenomenon will move manufacturers in the direction of smaller batteries unless battery storage capacity one day becomes negligible relative to energy costs. Of course, batteries generally need to be oversized to ensure adequate performance over the lifetime of the vehicle. Although a smaller battery might reduce the purchase price of a PHEV, it may incur higher maintenance costs because it undergoes deeper discharge cycles that can accelerate power and capacity fade [41].

2.4.2 SOC Range

To investigate the relationship between battery size and discharge depth, consider the distribution of SOC ranges shown in Fig. 2.8 for the two most extreme battery sizes (40 and 320 modules). Here we define SOC range as the difference between the maximum and minimum SOC values achieved during the drive cycle. The asymptote at 0.65 occurs because the control strategy limits SOC between 0.25 and 0.9 using exterior point penalty functions (see [38]). The 40-module battery reaches full discharge depth in between 10 and 20 minutes, whereas the 320-module battery reaches full discharge depth in between 55 and 80 minutes. Within 10 to 20 minutes, only 35-60% of trips in one day have terminated. Therefore, in 40-65% of daily trips, a 40-module battery will reach full depletion. On the other hand, within 55 to 80 minutes, 84-90% of trips have terminated, meaning only 10-16% of PHEV daily trips will result in full depletion of a 320-module battery. Since this percentage is relatively small in comparison to the remainder of the population, the benefits of large battery sizes diminish as the number of modules increases.

Figure 2.8 can also be used as an analysis tool to size batteries. For example, suppose we wish to specify a battery size that uses no more than half of the SOC range in 75 percent of daily trips. Reading off the cumulative probability curve, 75 percent of daily travel times are 32 minutes or less. Then we could populate Fig. 2.8 with the SOC range distribution for several battery sizes and determine which size achieves 0.5 SOC range or less for the first 32 minutes. Hence, Fig. 2.8 allows the design engineer to leverage simulation results to make battery sizing decisions based on rigorous arguments about SOC range and daily travel duration.

Eventually, it may make the most sense to treat PHEV battery size as an option on a vehicle, with

smaller batteries standard (for those in the majority of the population with relatively low daily travel needs) and larger batteries available at a premium to those with greater travel requirements.

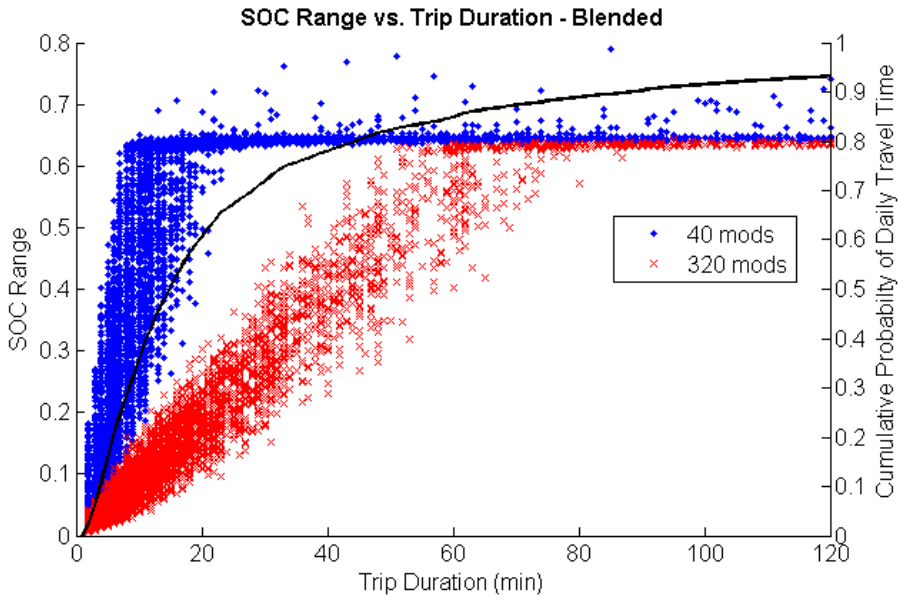

Figure 2.8: Distribution of SOC range for 40 and 320 modules, blended strategy. The solid line is the cumulative distribution of daily travel time (Fig. 2.4). CDCS has a similar distribution and is therefore omitted for brevity.

2.5 Conclusions

In this chapter we have introduced a method for evaluating power management strategies and battery energy capacity in PHEVs over a distribution of drive cycles and travel times. Through this framework, we have demonstrated that a blended control strategy facilitates the use of smaller batteries for a given operating cost or energy efficiency. We have also shown that expected operating cost and energy efficiency approach asymptotic values as battery size increases, since a very small population of drivers will fully deplete large batteries in one day. Because the effect that PHEV power management strategies will have on performance degradation and replacement time is not understood, this chapter has focused exclusively on optimizing energy cost. However, as scientific knowledge of PHEV battery performance and durability improve, it will be important to include these other factors into the power management objective function.

Chapter 3

Conclusions and Future Work

This thesis examines the supervisory power management control problem of optimally blending fuel and electricity in a plug-in hybrid electric vehicle (PHEV), and how these control laws, relate to battery size and overall performance. Through this effort, we have provided the following key contributions to the PHEV power management and battery sizing literature: First, this thesis formally derives optimal power management algorithms over a probability distribution of drive cycle behavior for PHEVs, rather than for a single cycle, using stochastic dynamic programming. Secondly, this work applies an economics inspired cost function to optimally balance the consumption cost of fuel vis-a-vis electricity. Thirdly, we use this formulation to analyze how varying energy purchase prices might impact optimal power management, in light of the historically volatile fluctuation of these values. This enables us to understand how to develop power management algorithms that are robust to these varying prices. Fourth, we use the Markov chain drive cycle modeling framework in conjunction with real-world daily trip length data to build stochastic models of daily drive cycles. This allows to simulate the closed-loop PHEV model across stochastic distributions of drive cycles, to obtain probability distributions of performance results. Finally, we apply the aforementioned PHEV model, stochastic daily drive cycle/trip length models, and power management algorithms to a range of battery sizes to understand how they all interact. The results indicate that optimal blending enables the use of smaller battery sizes, particularly for battery packs with less energy storage capacity.

This work has made significant contributions towards optimal control and design of PHEV powertrain systems, particularly with regard to the coupled problems of optimal blending and battery sizing. However, several important issues remain. Battery health dynamics are currently not understood very well, and can have a significant impact on PHEV performance, cost, safety, and durability. As a result, future work shall investigate first-principle models of battery health degradation currently being developed within our research group. These models will be validated on a simple experimental test bench, which will have the capability of loading the batteries in real-time along with our PHEV powertrain simulation models, in a

hardware-in-the-loop setup. Through this effort, we will obtain models that map battery cell operating characteristics to health degradation. The models will then inform an optimal control problem that seeks to management battery cell loads within a battery pack in a manner that minimizes degradation, rather than simply achieve charge equalization. With this algorithm in place, we can then return to the overall PHEV power management problem and include battery degradation in the form of maintenance cost as an additional term to energy consumption cost. As a result, the final set of results will represent a comprehensive modeling and control study on optimal PHEV power management with respect to energy consumption costs and battery health degradation.

Bibliography

[1] A. Shabashevich, D. Saucedo, T. Williams, C. Reif, C. Lattoraca, B. Jungers, B. Wietzel, A. Frank, and T. Fate, "Consumer Ready Plug-in Hybrid Electric Vehicle," *Team-Fate, University of California, Davis. http://www.teamfate.net/technical/UCDavis_Spring2007_TechReport.pdf*, 2007.

[2] J. Ronning, "The viable environmental car: The right combination of electrical and combustion energy for transportation," *SAE Paper 971629*, pp. 35–43, 1997.

[3] A. Simpson, "Cost-benefit analysis of plug-in hybrid electric vehicle technology," *Presented at the 22nd International Battery, Hybrid and Fuel Cell Electric Vehicle Symposium and Exhibition (EVS-22*, vol. NREL/CP-540-40485, 2006.

[4] G. Paganelli, G. Ercole, A. Brahma, Y. Guezennec, and G. Rizzoni, "General supervisory control policy for the energy optimization of charge-sustaining hybrid electric vehicles," *JSAE Review*, vol. 22, no. 4, pp. 511–518, 2001.

[5] C. Musardo, G. Rizzoni, Y. Guezennec, and B. Staccia, "A-ecms: An adaptive algorithm for hybrid electric vehicle energy management," *European Journal of Control*, vol. 11, no. 4-5, pp. 509–524, 2005, compilation and indexing terms, Copyright 2008 Elsevier Inc.

[6] A. Sciarretta, M. Back, and L. Guzzella, "Optimal control of parallel hybrid electric vehicles," *IEEE Transactions on Control Systems Technology*, vol. 12, no. 3, pp. 352–63, 05 2004.

[7] A. Brahma, Y. Guezennec, and G. Rizzoni, "Optimal energy management in series hybrid electric vehicles," in *Proceedings of 2000 American Control Conference (ACC 2000)*, vol. 1. Chicago, IL, USA: American Autom. Control Council, 28-30 June 2000 2000, pp. 60–4.

[8] C.-C. Lin, H. Peng, J. W. Grizzle, and J.-M. Kang, "Power management strategy for a parallel hybrid electric truck," *IEEE Transactions on Control Systems Technology*, vol. 11, no. 6, pp. 839–49, 11 2003.

[9] M. P. O'Keefe and T. Markel, "Dynamic programming applied to investigate energy management strategies for a plug-in hev," in *22nd International Battery, Hybrid and Fuel Cell Electric Vehicle Symposium, (EVS-22)*, October 23, 2006 2006.

[10] Q. Gong, Y. Li, and Z.-R. Peng, "Trip based optimal power management of plug-in hybrid electric vehicles using gas-kinetic traffic flow model," *American Control Conference, 2008*, pp. 3225–3230, June 2008.

[11] M. Koot, J. T. B. A. Kessels, B. de Jager, W. P. M. H. Heemels, P. P. J. van den Bosch, and M. Steinbuch, "Energy management strategies for vehicular electric power systems," pp. 771–782, 2005.

[12] A. Vahidi, A. Stefanopoulou, and H. Peng, "Current management in a hybrid fuel cell power system: A model-predictive control approach," *IEEE Transactions on Control Systems Technology*, vol. 14, no. 6, pp. 1047–1057, 2006.

[13] B. K. Powell, K. E. Bailey, and S. R. Cikanek, "Dynamic modeling and control of hybrid electric vehicle powertrain systems," *IEEE Control Systems Magazine*, vol. 18, no. 5, pp. 17–33, 10 1998.

[14] A. Kimura, T. Abe, and S. Sasaki, "Drive force control of a parallel-series hybrid system," *JSAE Review*, vol. 20, no. 3, pp. 337–341, 1999.

[15] D. Rizoulis, J. Burl, and J. Beard, "Control strategies for a series-parallel hybrid electric vehicle," *SAE Paper 2001-01-1351*, 2001.

[16] P. B. Sharer, A. Rousseau, D. Karbowski, and S. Pagerit, "Plug-in hybrid electric vehicle control strategy: Comparison between ev and charge-depleting options," *SAE Papers, 2008 SAE World Congress*, vol. 2008-01-0460, 2008.

[17] A. Rousseau, S. Pagerit, and D. Gao, "Plug-in hybrid electric vehicle control strategy parameter optimization," Electric Vehicle Symposium-23, Tech. Rep., 2007.

[18] N. J. Schouten, M. A. Salman, and N. A. Kheir, "Fuzzy logic control for parallel hybrid vehicles," *IEEE Transactions on Control Systems Technology*, vol. 10, no. 3, pp. 460–8, 05 2002.

[19] B. M. Baumann, G. Washington, B. C. Glenn, and G. Rizzoni, "Mechatronic design and control of hybrid electric vehicles," *IEEE/ASME Transactions on Mechatronics*, vol. 5, no. 1, pp. 58–72, 2000.

[20] D. Bertsekas, *Dynamic Programming and Optimal Control. Vol. 2.* Athena Scientific.

[21] I. . Kolmanovsky, I. Siverguina, and B. Lygoe, "Optimization of powertrain operating policy for feasibility assessment and calibration: stochastic dynamic programming approach," in *Proceedings of 2002*

American Control Conference, vol. 2. Anchorage, AK, USA: American Automatic Control Council, 8-10 May 2002 2002, pp. 1425–30.

[22] C.-C. Lin, "Modeling and Control Strategy Development for Hybrid Vehicles." Ph.D. dissertation, University of Michigan, Ann Arbor, 2004.

[23] J. Liu and H. Peng, "Modeling and control of a power-split hybrid vehicle," *Control Systems Technology, IEEE Transactions on*, vol. 16, no. 6, pp. 1242–1251, Nov. 2008.

[24] E. Tate, "Techniques for hybrid electric vehicle controller synthesis," *Electrical Engineering: Systems, University of Michigan, Ann Arbor, Michigan*, 2007.

[25] L. Johannesson, M. Asbogard, and B. Egardt, "Assessing the potential of predictive control for hybrid vehicle powertrains using stochastic dynamic programming," *Intelligent Transportation Systems, IEEE Transactions on*, vol. 8, no. 1, pp. 71–83, 2007.

[26] K. Muta, M. Yamazaki, and J. Tokieda, "Development of new-generation hybrid system ths ii-drastic improvement of power performance and fuel economy," *SAE Paper 2004-01-0064*, 2004.

[27] S. J. Moura, D. S. Callaway, H. K. Fathy, and J. L. Stein, "Impact of battery sizing on stochastic optimal power management in plug-in hybrid electric vehicles," *Vehicular Electronics and Safety, 2008. ICVES 2008. IEEE International Conference on*, pp. 96–102, Sept. 2008.

[28] K. B. Wipke, M. R. Cuddy, and S. D. Burch, "Advisor 2.1: A user-friendly advanced powertrain simulation using a combined backward/forward approach," *IEEE Transactions on Vehicular Technology*, vol. 48, no. 6, pp. 1751–1761, 1999.

[29] V. H. Johnson, "Battery performance models in advisor," *Journal of Power Sources*, vol. 110, no. 2, pp. 321–329, 2002.

[30] Anonymous, "Annual energy review," no. DOE/EIA-0384(2006), June 2007. [Online]. Available: http://www.eia.doe.gov/aer/

[31] P. Papalambros and D. Wilde, *Principles of Optimal Design: Modeling and Computation, 2nd Ed.* Cambridge University Press, 2000.

[32] J. Gubner, *Probability and Random Processes for Electrical and Computer Engineers.* Cambridge University Press, 2006.

[33] T. W. Anderson and L. A. Goodman, "Statistical inference about markov chains," *Annals of Mathematical Statistics*, vol. 28, no. 1, pp. 89–110, 1957.

[34] W. Kempton and J. Tomic, "Vehicle-to-grid power fundamentals: Calculating capacity and net revenue," *Journal of Power Sources*, vol. 144, no. 1, pp. 268–279, 2005.

[35] T. Markel and A. Simpson, "Energy storage systems considerations for grid-charged hybrid electric vehicles," p. 6, 2005.

[36] A. F. Burke, "Batteries and ultracapacitors for electric, hybrid, and fuel cell vehicles," *Proceedings of the IEEE*, vol. 95, no. 4, pp. 806–20, 04 2007.

[37] P. B. Sharer, A. Rousseau, S. Pagerit, and P. Nelson, "Midsize and suv vehicle simulation results for plug-in hev component requirements," *SAE Papers, 2007 SAE World Congress*, vol. 2007-01-0295, 2007.

[38] S. J. Moura, H. K. Fathy, D. S. Callaway, and J. L. Stein, "A stochastic optimal control approach for power management in plug-in hybrid electric vehicles," *ASME Dynamic Systems and Control Conference*, Sept. 2008.

[39] J. Douglas, "Plug-in hybrids on the horizon: Building a business case," *EPRI Journal*, p. 10, 2008.

[40] M. Verbrugge and E. Tate, "Adaptive state of charge algorithm for nickel metal hydride batteries including hysteresis phenomena," *Journal of Power Sources*, vol. 126, no. 1-2, pp. 236–249, 2004.

[41] G. L. Plett, "Extended kalman filtering for battery management systems of lipb-based hev battery packs. part 1. background," *Journal of Power Sources*, vol. 134, no. 2, pp. 252–61, 08/12 2004.

[42] P. Brockwell and R. Davis, *Time Series: Theory and Methods*. Springer, 1998.